Received: 17 May 2023 | Revised: 9 August 2023 | Accepted: 23 August 2023

DOI: 10.1002/ctpp.202300064

ORIGINAL ARTICLE

Contributions to Plasma Physics

# Effect of elastic scattering between ions and neutral particles on ion transport perpendicular to magnetic fields in divertor plasmas

**Daisuke Umezaki**[1] | **Hideaki Matsuura**[1] | **Kazuo Hoshino**[2]

[1]Department of Applied Quantum Physics and Nuclear Engineering, Kyushu University, Fukuoka, Japan

[2]Faculty of Science and Technology, Keio University, Yokohama, Kanagawa, Japan

**Correspondence**
Daisuke Umezaki, Department of Applied Quantum Physics and Nuclear Engineering, Kyushu University, Motooka, Fukuoka 819-0395, Japan.
Email: umezaki.daisuke.786@s.kyushu-u.ac.jp

**Funding information**
Japan Science and Technology Agency, Grant/Award Number: JPMJSP2136

**Abstract**

In divertor plasmas, atomic processes play a significant role in reducing the divertor heat load. In particular, the elastic scattering between ions and neutral particles can be characterized as a large-angle scattering; this is in contrast with Coulomb scattering, which is dominated by small-angle scattering. In a large-angle scattering, a large fraction of the ion energy is transferred to the neutral particle, and the particle flight direction can be changed significantly. This process can generate additional particle transport perpendicular to magnetic field lines and affect plasma density profile in neutral-rich divertor regions. However, in most edge plasma simulation codes, the elastic scattering with neutral particles is not taken into account in the direction perpendicular to the magnetic field lines. In this study, we performed a 2D orbital calculation without other drifts such as diamagnetic and $E \times B$ drifts to assess the effect of the elastic scattering on the density profile. The peak density is found to be decreased by 11.1 (6.3)% compared with the model that ignores the transport due to the elastic scattering, even at 3.0 (5.0) T magnetic field similar to that of the JT-60SA (JA DEMO reactor) class. In addition, the ion transport can be expressed as a diffusion model by integrating the differential cross section over the large-angle scattering range $\pi/2 - \pi$. The proposed method may be easily introduced into any integrated codes to consider the elastic scattering.

**KEYWORDS**

divertor, elastic scattering, ion transport, large-angle scattering

## 1 | INTRODUCTION

To realize a functional fusion reactor, reducing the divertor heat load is one of the most critical aspects that need to be addressed. A detached divertor will be employed to reduce the divertor heat load in many fusion devices, including ITER, JT-60SA, and Japan's DEMO reactor. The establishment of detached divertor is important, and it requires enhancement of the power radiation due to impurity injection and interactions between plasmas and neutrals. The interactions between ions and neutral particles, such as charge exchange and elastic scattering, help ion diffusion. Additionally, impurity power radiation reduces electron temperature and facilitates volume recombination. The DEMO reactor needs to radiate 80% of inflowing power into edge plasmas from the core plasma to achieve a heat load peak of less than 10 MW $m^{-2}$.[1]

  

In detached divertor plasmas, the momentum and energy loss for ions caused by the interactions between ions and neutral particles, such as elastic scatterings, play a crucial role. Our previous study[2] indicated that ions are transported in the radial direction by large-angle elastic scattering between deuterons and deuterium atoms, although the magnetic field was ignored. In that study, the plasma was treated by a fluid model, and background neutral particle density was assumed as be a constant multiple of plasma density. In this present study, an orbital calculation model is employed to consider magnetic fields and to treat ion motion kinetically. Additionally, a neutral particle density profile is simulated using a simplified fluid model.

From a quantum point of view, it is impossible to distinguish the elastic scattering from charge exchange between identical nuclei, such as a deuteron and a deuterium atom.[3,4] Therefore, we consider the elastic scattering cross section with no further consideration of the charge exchange in a classical sense. Hence, in this paper, "the scattering process involving the elastic scattering and charge exchange between deuteron and deuterium atom" will simply be written as "the elastic scattering." As will be shown in a next section, the elastic scattering occurs not only at small-angle scattering but also at large-angle scattering. In a large-angle scattering, a large fraction of the ion/neutral energy is transferred from the neutrals/ions, and the particle flight direction can be changed significantly during a single scattering event. It is crucial to appropriately consider the large-angle elastic scattering in divertor plasma regions with abundant neutral particles. Ions and neutral particles reach temperature equilibrium through the elastic scattering. In this study, the neutral temperature is proposed to be equal to the ion temperature. Movement of a guiding center via momentum exchange plays an important role in the transport effect discussed in this study.

Various codes have been developed to simulate edge plasmas, including plasma fluid codes (e.g., B2,[5] B2.5,[6] SOLDOR,[7,8] and EMC3[9–11]), neutral particle transport Monte Carlo (MC) codes (e.g., EIRENE,[4,12–14] NEUT2D,[7,8] and DEGAS 2[15]), and fluid or MC transport codes for impurities. Integrated codes typically consist of a plasma fluid code, a neutral fluid/MC code, and an impurity fluid/MC code. There are some well-known integrated codes such as the SOLPS,[16] SOLPS-ITER,[17,18] SONIC,[19,20] EMC3-EIRENE,[9–11] UEDGE-EIRENE[21–23] so forth, and the relationships between each code and integrated code are shown in Figure 1. Most of integrated codes compute the momentum conservation equation for plasmas along the direction parallel to the magnetic field lines. For instance, the SONIC code[19,20] assumes the radial ion transport only due to the anomalous diffusion, which is adjusted to reproduce the experimental results as much as possible. The code has been employed the analyses of the JT-60U experiment[24]; however, the density profile at the outer divertor plates was overestimated by a factor of 2–3. Enhancement of the radial transport by the large-angle elastic scattering may improve the result and also may affect design study of JA DEMO reactor.[25,26] In the SOLPS code, the large-angle elastic scattering is taken into account. However, how the elastic scattering affects the plasma transport in the direction perpendicular to magnetic field lines, especially in the detachment, has not been investigated in detail.

Particle-in-cell (PIC) models are effective for studying ion kinetics in edge plasmas. Several PIC codes, including BIT1 code[27–29] and PARASOL code,[30–32] have been developed and have produced significant results in investigating the magnetized plasma-wall-transition layer and drift effects. The BIT1 code simulates plasmas in one spatial and three velocity dimensions and assumes isotropic elastic scattering between ions and neutrals. However, the one-dimensional spatial model such as the BIT1 code cannot account for particle transport perpendicular to the magnetic field lines. On the other hand, the PARASOL code traces ions in a two-dimensional space, considers $\vec{E} \times \vec{B}$ drift movement, and assumes isotropic elastic scattering.

Therefore, it is important to assess the impact of elastic scattering on plasma transport perpendicular to magnetic field lines. This study aims to assess the effect of elastic scattering between deuterons and deuterium atoms on ion transport

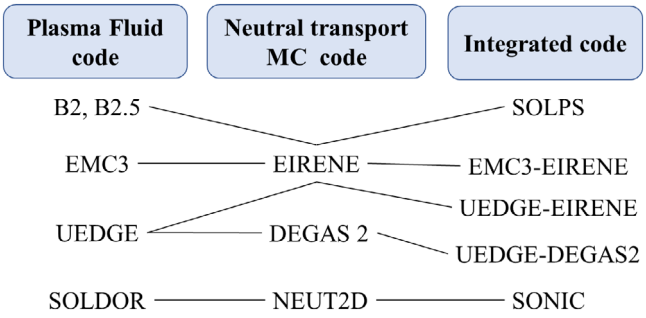


**FIGURE 1** Relationship between plasma fluid codes and neutral transport Monte Carlo codes.

and density profiles using an orbital calculation in a 2D space. Furthermore, we propose a diffusion model to reproduce the transport effect due to the elastic scattering, which may be easily introduced into the existing integrated codes.

## 2 | ANALYSIS MODEL

In this study, two methods for dealing with ion transport are employed. The first approach involves a kinetic simulation of an ion guiding center movement due to scatterings, as described later. When the elastic scattering occurs, a velocity and guiding center after the scattering are calculated considering the differential cross section. Figure 2 depicts the differential cross section of elastic scattering between deuterons and deuterium atoms in black, red, and blue lines.[3] Here, $E_{\mathrm{CM}}$ represents the center of mass collision energy and $\theta_{\mathrm{CM}}$ is the scattering angle in the center of mass system. Additionally, the Coulomb scattering cross section between deuterons and tritons is also shown in a green line. As shown in the differential cross section illustrated in Figure 2, the elastic scattering involves not only small-angle scattering but also large-angle scattering. The second approach involves computing movement of an ion guiding center due to scatterings using an MC method with a diffusion coefficient. To assess the impact of elastic scattering on ion transport, four simulation cases (A–D) are performed. Details of the simulation methods are explained in the subsequent section.

### 2.1 | Treatment of elastic scattering in the orbital calculation

When the elastic scattering occurs, the velocity of the neutral particle is selected from an isotropic Maxwellian distribution as the scattering partner. The velocity of the ion after scattering is determined by considering the differential cross section. The scattering angle is calculated in the same way as Ref. [33] to take the differential cross section into account. According to the treatment developed by our research group,[34–40] the new velocity of the scattered ion is calculated using Equation (1) and is shown in Figure 3.

$$\vec{v}_{\mathrm{i}} = \vec{V}_{\mathrm{G}} + \vec{V}_{\mathrm{i}} \cos\theta_{\mathrm{CM}} + \left|\vec{V}_{\mathrm{i}}\right| \vec{s} \sin\theta_{\mathrm{CM}}. \tag{1}$$

$$\vec{s} = \frac{1}{\sqrt{V_{ix}^2 + V_{iy}^2}} \begin{pmatrix} V_{iy}\cos\xi_{\mathrm{CM}} + \frac{V_{ix}V_{iz}\sin\xi_{\mathrm{CM}}}{V_{\mathrm{i}}} \\ -V_{ix}\cos\xi_{\mathrm{CM}} + \frac{V_{iy}V_{iz}\sin\xi_{\mathrm{CM}}}{V_{\mathrm{i}}} \\ -\left(V_{ix}^2 + V_{iy}^2\right)\frac{\sin\xi_{\mathrm{CM}}}{V_{\mathrm{i}}} \end{pmatrix}. \tag{2}$$

In Equations (1) and (2), $\vec{v}_{\mathrm{i}}$ is the new ion velocity after the scattering event, $\vec{V}_{\mathrm{G}}$ is the velocity of the center of mass, $\theta_{\mathrm{CM}}$ is the scattering angle of the center of mass, $\vec{V}_{\mathrm{i}} = \left(V_{ix}, V_{iy}, V_{iz}\right)$ is the ion velocity before the scattering in

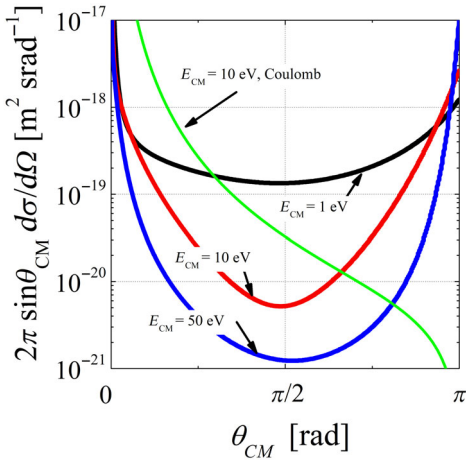


**FIGURE 2** Differential cross section $2\pi \sin\theta_{\mathrm{CM}} d\sigma/d\Omega$ of the elastic (Coulomb) scattering between deuteron and deuterium (triton).

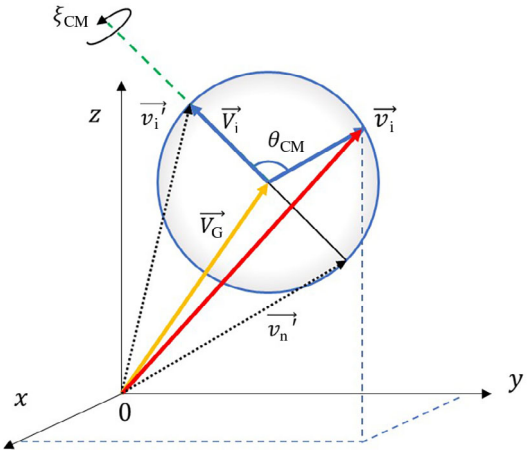


**FIGURE 3** Schematic of the change in the ion velocity before and after elastic scattering.

the center of mass system ($\vec{V}_i = \vec{v_i}' - \vec{V}_G$), and $\vec{s}$ is a unit vector perpendicular to $\vec{V}_i$. The component of parallel (perpendicular) to the magnetic field of $\vec{v}_i$ is $v_\parallel$ ($v_\perp$). These equations can be obtained from the conservation of energy and momentum. Using the rotation angle $\varphi_{rot} = 2\pi \times r_G$, the ion velocity before the scattering $\vec{v_i}'$ can be expressed as $\vec{v_i}' = \left(v_\parallel, v_\perp \sin\varphi_{rot}, -v_\perp \cos\varphi_{rot}\right)$. In the velocity space, the velocity after elastic scattering lies on the surface of a sphere with radius $\left|\vec{V}_i\right|$. The center of the sphere is located at the end of the $\vec{V}_G$ vector. $\xi_{CM}$ is the angle around the axis along with $\vec{V}_i$ and is determined in the range of $0 \le \xi_{CM} \le 2\pi$ using a uniform random number. $\theta_{CM}$ is determined by considering the differential cross section of the elastic scattering. This method can be used to determine the velocity after each elastic scattering event if the velocities of the two particles before scattering and the differential cross section are known. When the elastic scattering occurs, the ion position before the scattering is calculated as $\left(x', y' + r'_L \cos\varphi_{rot}, r'_L \sin\varphi_{rot}\right)$ using the rotation angle $\varphi_{rot} = 2\pi \times r_G$ on the rotational orbit. The new position of guiding center $(x, y, z)$ after the scattering can be obtained from the new velocity $\vec{v}_i$ as follows:

$$\begin{pmatrix} x \\ y \\ z \end{pmatrix} = \begin{pmatrix} x' + r_L \times F_x/|\vec{F}| \\ y' + r'_L \cos\varphi_{rot} + r_L \times F_y/|\vec{F}| \\ r'_L \sin\varphi_{rot} + r_L \times F_z/|\vec{F}| \end{pmatrix}, \tag{3}$$

where $r_L = m\left|\vec{v}_i\right|/qB$ ($r'_L$) is the Larmor radius after (before) the scattering, $\vec{F} = \left(F_x, F_y, F_z\right) = q\vec{v}_i \times \vec{B}$ is the Lorentz force; however, the movement in the $z$-axis direction is ignored and the orbit calculation is continued using the new guiding center position $(x, y)$. The position of the guiding center is tracked during the orbital calculation. When the elastic scattering occurs or when the density is calculated by the orbital particle, the particle's position on the Larmor orbit is determined using a uniform random number. A velocity and guiding center position after the elastic scattering are calculated using Equations (1–3). In the simulation of case A, the elastic scattering and anomalous diffusion are considered as a cause of movement of an ion guiding center. The distance traveled in the perpendicular direction to the magnetic field due to anomalous diffusion is expressed as $\Delta y = \sqrt{2D_a\Delta t} \times r_G$, where $\Delta t$ is the time step interval and $r_G$ is a normal random number. The anomalous diffusion coefficient $D_a$ is 0.3 $m^2\ s^{-1}$ with reference to other previous works.[24–26] On the other hand, in case B, although the velocity is calculated from Equations (1) and (2), the movement of guiding center in the direction perpendicular to magnetic fields is ignored. In other words, Equation (3) is not used.

## 2.2 | Treatment of the elastic scattering as a diffusion

To incorporate the transport effect of the elastic scattering into the diffusion coefficient, we calculated it as follows:

$$D_{EL} = r_L^2 \langle\sigma v\rangle_{EL} n_n, \tag{4}$$

where $\langle\sigma v\rangle_{EL}$ is the reaction rate coefficient obtained from the cross section in Ref. [3]. The expression of Equation (4) is often used and is the product of the reaction rate coefficient and the collision frequency.

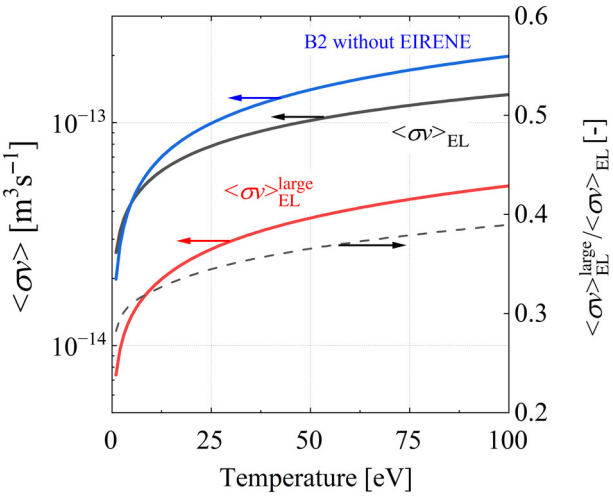


**FIGURE 4** Relationship between each reaction rate coefficient and temperature.

**TABLE 1** Characteristics of each simulation case.

| | Case A | Case B | Case C | Case D |
|---|---|---|---|---|
| Elastic scattering | Considered by the kinetic way | Ignored | Considered using the diffusion coefficient | |
| Diffusion coefficient | $D_a$ | $D_a$ | $D_a + D_{EL}$ | $D_a + D_{EL}^{large}$ |

However, as described in Section 1, the large-angle elastic scattering dominates the change in ion flight direction, indicating Equation (4) may overestimate the transport effect due to the elastic scattering. Therefore, we calculated a new cross section by integrating the differential cross section over the large-angle range of $\pi/2$ to $\pi$ and obtained an additional reaction rate coefficient $\langle\sigma v\rangle_{EL}^{large}$. This diffusion coefficient due to the large-angle elastic scattering is expressed as follows:

$$D_{EL}^{large} = r_L^2 \langle\sigma v\rangle_{EL}^{large} n_n. \tag{5}$$

Using Equations (4) or (5), the distance traveled in the perpendicular direction of magnetic field can be written as $\Delta y = \sqrt{2(D_a + D_{EL})\Delta t} \times r_G$ or $\Delta y = \sqrt{2\left(D_a + D_{EL}^{large}\right)\Delta t} \times r_G$. Figure 4 shows the reaction rate coefficients $\langle\sigma v\rangle_{EL}$ and $\langle\sigma v\rangle_{EL}^{large}$ represented by the black and red lines, respectively. For reference, a reaction rate coefficient utilized in the B2 code, when the code is combined with a neutral fluid model without simulating the EIRENE, is also shown by the blue line.[6] On the right axis, a ratio $\langle\sigma v\rangle_{EL}^{large}/\langle\sigma v\rangle_{EL}$ is presented as a black dotted line. As can be seen from the figure, the large-angle scattering accounts for approximately 30%–40% of the total elastic scattering.

In simulation cases C and D, the elastic scattering is taken into account as a diffusion coefficient. The former $\Delta y$ is for simulation case C and the latter is for case D. In these simulation cases, the movement of guiding center is considered as above diffusion, and Equation (3) is not used.

In summary, the four orbital simulation cases (cases A–D) are performed. The characteristics of these simulation cases are summarized in Table 1.

## 2.3 | Background conditions

Figure 5 illustrates a simplified 2D scheme ($100 \times 20$ cm$^2$) of a tokamak divertor region, where the $x$-axis is aligned parallel to the magnetic field $\vec{B}$. The $y$-axis is perpendicular to the $x$-axis and parallel to the divertor plates, while the $z$-axis is perpendicular to both the $x$- and $y$-axes. Moreover, the uniform magnetic field is assumed from the upwind boundary to the divertor plate, with $B_T$ and $B_P$ values of 3.0–5.0 and 0.2 T. The chosen magnetic field conditions of $B_T = 3.0$ and 5.0 T approximately correspond to the magnetic fields of JT-60SA and JA DEMO reactor, respectively.

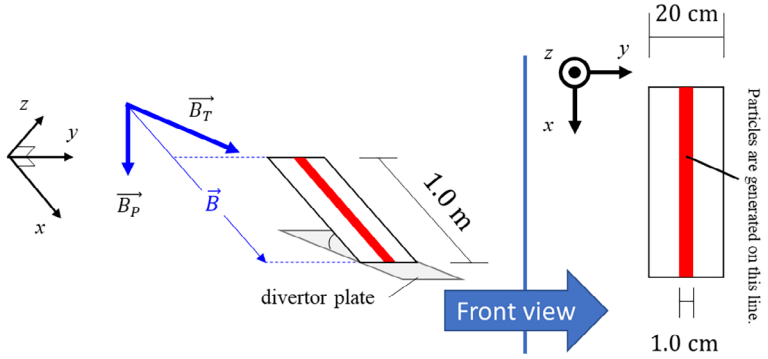


**FIGURE 5** Calculation scheme with reference to the divertor plasma region.

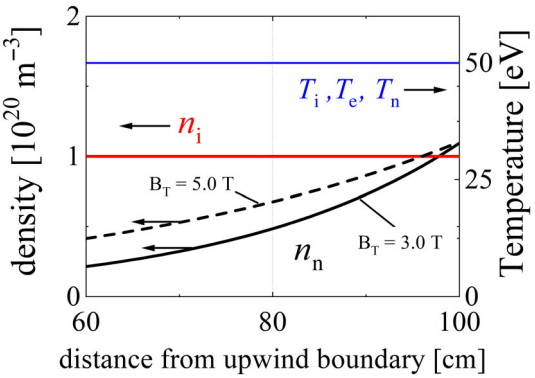


**FIGURE 6** Background plasma parameters for an orbital simulation.

To adequately assess the effect of the elastic scattering on ion transport, an orbital calculation for deuterons is performed in fixed background plasmas using the track-length estimator method as a scoring technique to simulate the ion density.[41] The orbital particles are generated along a line up to 100 cm from the divertor plate and a width of 1 cm. The width of 1.0 cm corresponds roughly to width of a cell in the SONIC code. The guiding center position $(x, y)$ is traced in the 2D space, ignoring the movement of guiding center in the $z$-axis. Moreover, the effects of Coulomb scattering, frictional force, and the anomalous diffusion on the orbital ions are treated in the same way as in the IMPMC code.[42–44]

The background particles considered in the simulation are deuterons, electrons, and deuterium atoms. For clear assessment of the elastic scattering effect, complex physics discussions such as $E \times B$ drift and plasma blob transport are excluded from the analysis. The background plasma parameters, including plasma density $n_i$, ion temperature $T_i$, and electron temperature $T_e$, are fixed at $1 \times 10^{20}$ m$^{-3}$, 50 eV, and 50 eV, respectively, based on the SONIC simulation results.[25,26] These are the values at the divertor plate of JA DEMO reactor near a peak of heat load. Temperature and density plateaued in a width of about a few cm; hence, the background values are chosen as representative conditions. The neutral particle density profile is simulated in the same way as in Ref. [45] using the reflection coefficient in Ref. [46], and the neutral temperature $T_n$ is assumed to be equal to the ion temperature. The background plasma flow velocity $v_f$ is set to $1.0 \times 10^4$ m s$^{-1}$. Figure 6 shows the background ion density $n_i$, neutral density $n_n$, ion, electron, and neutral temperature $T_i$, $T_e$, $T_n$ and flow velocity $v_f$ from the upwind boundary to the divertor plate. Furthermore, the elastic scattering and the recombination are considered for orbital ions as atomic processes, and their occurrences are calculated in the same way as in the IMPMC code.

## 3 | NUMERICAL RESULT

To assess the effect of elastic scattering on the density profile, we performed the orbital simulation in the simplified 2D scheme described in Section 2. Figure 7a,b depicts the density profiles at the divertor plate for two cases: case A considers

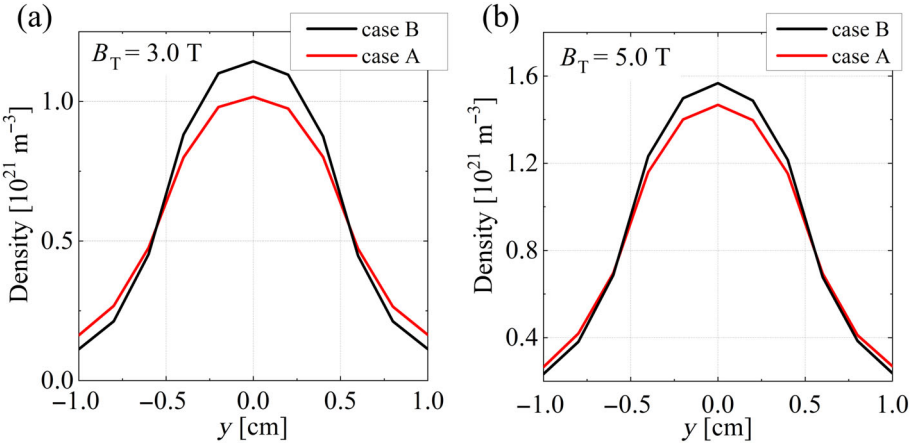


**FIGURE 7** Density profiles at the divertor plate for cases A and B (Guiding center movement ignored) at $B_T = 3.0$ and 5.0 T.

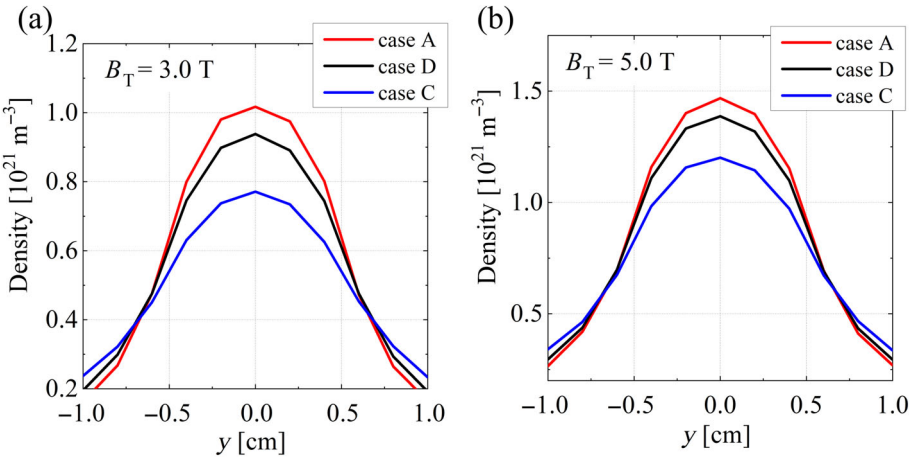


**FIGURE 8** Density profiles at the divertor plate for cases A, C, and D at $B_T = 3.0$ and 5.0 T.

the elastic scattering, case B ignores the movement of the guiding center due to the elastic scattering at $B_T = 3.0$ and 5.0 T, respectively. The peak densities at $B_T = 3.0$ T for the cases A and B are 1.02 and $1.14 \times 10^{21}$ m$^{-3}$, respectively. It is found that the density profile was broadened by the elastic scattering and the peak density in case A was reduced by 11.1% compared with case B. Similarly, at $B_T = 5.0$ T, the peak density in cases A and B are 1.47 and $1.57 \times 10^{21}$ m$^{-3}$; hence, the peak value reduced by 6.3%. Although these magnetic field strengths correspond to those of JT-60SA and JA DEMO reactors, the effect of the elastic scattering on ion transport in the direction perpendicular to the magnetic field is not taken into account in the SONIC code, just like with case B. Therefore, we believe that it can be worth considering the ion transport perpendicular to the magnetic field due to the elastic scattering in the SONIC code for simulating future fusion devices.

Figure 8a,b shows the density profile at the divertor plate for cases A, C, and D. Cases C and D used the diffusion coefficients from Equations (4) and (5), respectively, at magnetic field strengths of 3.0 and 5.0 T. The peak densities for cases A, C, and D at $B_T = 3.0\,(5.0)$ T are 1.02, 0.77, and 0.94 (1.47, 1.20 and 1.39) $\times 10^{21}$ m$^{-3}$, respectively. Comparing case C with case A, as expected in Section 2, the peak density was underestimated than case A by $-24.2\,(-18.2)$ % at $B_T = 3.0\,(5.0)$ T. This is because, the reaction rate coefficient in Equation (4) is calculated using the cross section that is the integrated value of differential cross section over all scattering angles. In fact, the large-angle elastic scattering dominates the ion transport perpendicular to magnetic fields. Comparing the results of case D with case A, it is found that the peak density was underestimated by $-7.75$ $(-5.52)$% at $B_T = 3.0$ (5.0) T than case A. By taking only the large-angle elastic scattering into account, the density profile approached the result of case A. Therefore, it may be possible to introduce the effect of the elastic scattering on ion transport into integrated codes by calculating the diffusion coefficient using Equation (5).

As shown in Figure 4, approximately 60%–70% of the reaction rate coefficient calculated using the total cross section derives from small-angle regions. If the reaction rate coefficient obtained from the total cross section is utilized to calculate the diffusion coefficient, it incorporates even small-angle scatterings, which contribute little to ion transport. As a result, the effect of the elastic scattering on ion transport is overestimated. One possible way to improve the accuracy of the transport model using the diffusion coefficient due to the elastic scattering is to determine the range of large-angle scattering, which would bring the results closer to those obtained in case A. However, identifying this range could be challenging as the differential cross section depends on collision energy. At least for the background plasma assumed in this study, the overestimation of the transport effect due to the elastic scattering can be avoided using Equation (5).

Figure 9 shows the dependence of the coefficients of diffusion induced by the elastic scattering on $T_i$ (= $T_n$) and $n_n$. Figure 9a,c displays the diffusion coefficients obtained using Equation (4) at $B_T = 3.0$ and 5.0 T, respectively. Similarly, Figure 9b,d shows the diffusion coefficients calculated using Equation (5) at $B_T = 3.0$ and 5.0 T, respectively. As shown in Figure 9b, at the plasma conditions assumed in this study simulation such as $T_i \sim 50$ eV and $n_n \sim 0.5 \times 10^{20}$ m$^{-3}$, the diffusion coefficient is approximately 0.3 m$^2$ s$^{-1}$. Conversely, the result shown in Figure 9a is 1.0 m$^2$ s$^{-1}$, which is an overestimation of three times compared with that of Figure 9b. Similar trends can be seen in the results between Figure 9c,d. Moreover, the impact of the elastic scattering on ion transport is expected to be more significant in high-temperature and high-density neutral particles.

Furthermore, drift velocities such as diamagnetic drift and $E \times B$ drift depend on a plasma pressure, electric and magnetic field. These drifts have directional characteristics and typically have magnitude on the order of 1 km s$^{-1}$ in the poloidal direction and 0.1 km s$^{-1}$ in the radial direction.[47,48] As shown in this study, the perpendicular ion transport due to the elastic scattering broadens the plasma density profile. This transport may contribute to the ion movement from higher density regions to lower density regions. However, in this study, an isotropic neutral particle velocity distribution function was assumed. If the neutral particles have an anisotropic velocity distribution, such as a sifted-Maxwellian with a flow velocity in a specific direction, the transport due to elastic scattering may exhibit directional characteristics as well.

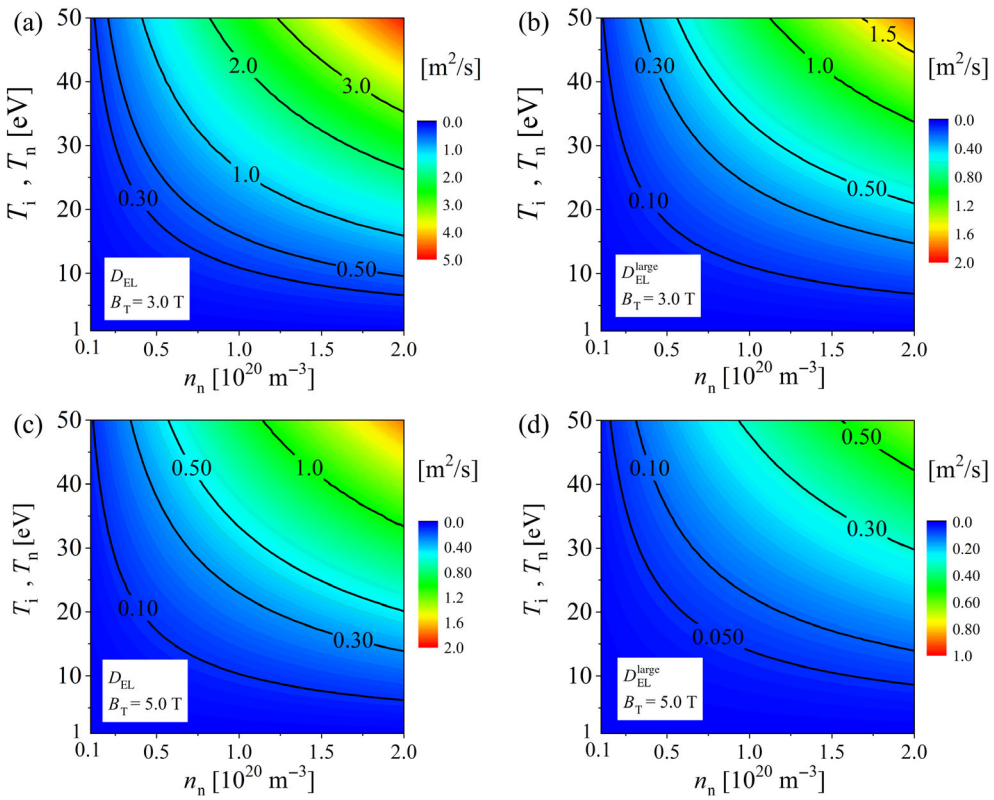


**FIGURE 9** Diffusion coefficients of the elastic scattering calculated from (a) Equation (4) at $B_T = 3.0$ T, (b) from Equation (5) at $B_T = 3.0$ T, (c) from Equation (4) at $B_T = 5.0$ T, and (d) from Equation (5) at $B_T = 5.0$ T.

## 4 | CONCLUSION

The effect of elastic scattering between deuteron and deuterium atom on ion transport and density profile was investigated using an orbital calculation in the simplified 2D scheme. The peak density was reduced due to the ion transport induced by the large-angle elastic scattering. In addition, the dependence of ion transport on magnetic field strengths assumed for JT-60SA and JA DEMO reactors was also investigated. At $B_T = 3.0$ (5.0) T, the peak density was reduced by 11.1% (6.3%) compared with the simulation case that ignored the guiding center movement due to the elastic scattering such as most of integrated codes. Moreover, we also attempted to express the transport included in the elastic scattering as the diffusion coefficient. The diffusion coefficient is calculated from the reaction rate coefficient and collision frequency based on a simple assumption. When the reaction rate was calculated using the cross section that the integral of the differential cross section over all scattering angles, the effect of elastic scattering on ion transport perpendicular to the magnetic field was overestimated. Using the cross section integrated over only large angles, the density profile approached to the result of the orbital simulation case, which considered the guiding center movement due to the elastic scattering. Therefore, it may be possible to incorporate the effect of the elastic scattering into integrated codes that ignores the elastic scattering in the direction perpendicular to the magnetic field lines, by utilizing the proposed method.

In this study, the background parameters for the orbit calculation were assumed to be constant and other complex physics such as $E \times B$ drift were ignored. To validate our findings regarding the large-angle elastic scattering effect on ion transport, it is necessary to introduce our model into an integrated code, such as SONIC, and perform a self-consistent integrated analysis. Furthermore, the effect of elastic scatterings between ions and molecules on ion transport in a radial direction will be assessed in future work.

## ACKNOWLEDGMENTS

This work was supported by JST SPRING, Grant Number JPMJSP2136.

## DATA AVAILABILITY STATEMENT

Research data are not shared.

## REFERENCES

[1] K. Hoshino, N. Asakura, S. Tokunaga, Y. Homma, K. Shimizu, Y. Sakamoto, K. Tobita, *Fusion Eng. Des.* **2017**, *124*, 352.
[2] D. Umezaki, H. Matsuura, *Plasma Fusion Res.* **2021**, *16*, 2403021.
[3] P. S. Kristié, D. R. Schultz, *At. Plasma-Mat. Interact. Data Fusion* **1992**, *8*, 1.
[4] R. E. Clark, in *Nuclear Fusion Research: Understanding Plasma-surface Interactions* (Eds: R. E. H. Clark, D. H. Reiter), Springer-Verlag, Berlin Heidelberg **2005**.
[5] B. J. Braams, N. E. T. Rep, *EURFU. XII-80/87/68*, Vol. 87, CEC, Brussels **1987**, p.68.
[6] R. Schneider, X. Bonnin, K. Borrass, D. P. Coster, H. Kastelewicz, D. Reiter, V. A. Rozhansky, B. J. Braams, *Contrib. Plasma Phys.* **2006**, *46*, 3.
[7] K. Shimizu, T. Takizuka, S. Sakurai, H. Tamai, H. Takenaga, H. Kubo, Y. Miura, *J. Nucl. Mater.* **2003**, *313*, 1277.
[8] H. Kawashima, K. Shimizu, T. Takizuka, N. Asakura, H. Takenaga, T. Nakano, S. Sakurai, *J. Nucl. Mater.* **2007**, *363*, 786.
[9] Y. Feng, F. Sardei, J. Kisslinger, P. Grigull, *J. Nucl. Mater.* **1997**, *241*, 930.
[10] Y. Feng, F. Sardei, J. Kisslinger, *J. Nucl. Mater.* **1999**, *266*, 812.
[11] Y. Feng, F. Sardei, J. Kisslinger, P. Grigull, K. McCormick, D. Reiter, *Contrib Plasma Phys.* **2004**, *44*, 57.
[12] D. Reiter, *J. Nucl. Mater.* **1992**, *196*, 80.
[13] D. Reiter, C. May, D. Coster, R. Schneider, *J. Nucl. Mater.* **1995**, *220*, 987.
[14] D. Reiter, M. Baelmans, P. Börner, *Fusion Sci. Technol.* **2005**, *47*, 172.
[15] D. P. Stotler, C. Karney, *Contrib. Plasma Phys.* **1994**, *34*, 392.
[16] A. S. Kukushkin, H. D. Pacher, V. Kotov, G. W. Pacher, D. Reiter, *Fusion Eng. Des.* **2011**, *86*, 2865.
[17] S. Wiesen, D. Reiter, V. Kotov, M. Baelmans, W. Dekeyser, A. S. Kukushkin, S. W. Lisgo, R. A. Pitts, V. Rozhansky, G. Saibene, I. Veselova, S. Voskoboynikov, *J. Nucl. Mater.* **2015**, *463*, 480.
[18] X. Bonnin, W. Dekeyser, R. Pitts, D. Coster, S. Voskoboynikov, S. Wiesen, *Plasma Fusion Res.* **2016**, *11*, 1403102.
[19] H. Kawashima, K. Shimizu, T. Takizuka, S. Sakurai, T. Nakano, N. Asakura, T. Ozeki, *Plasma Fusion Res.* **2006**, *1*, 31.
[20] K. Shimizu, T. Takizuka, K. Ohya, K. Inai, T. Nakano, A. Takayama, H. Kawashima, K. Hoshino, *Nucl. Fusion.* **2009**, *49*, 3403070.
[21] T. D. Rognlien, J. L. Milovich, M. E. Rensink, G. D. Porter, *J. Nucl. Mater.* **1992**, *196*, 347.
[22] T. D. Rognlien, P. N. Brown, R. B. Campbell, T. B. Kaiser, D. A. Knoll, P. R. McHugh, G. D. Porter, M. E. Rensink, G. R. Smith, *Contrib. Plasma Phys.* **1994**, *34*, 362.
[23] T. D. Rognlien, G. D. Porter, D. D. Ryutov, *J. Nucl. Mater.* **1999**, *266*, 654.

[24] K. Hoshino, K. Shimizu, T. Takizuka, N. Asakura, T. Nakano, *J. Nucl. Mater.* **2015**, *463*, 573.
[25] N. Asakura, K. Hoshino, S. Kakudate, F. Subba, C. Vorpahl, Y. Homma, H. Utoh, Y. Someya, Y. Sakamoto, R. Hiwatari, S. Suzuki, J. H. You, M. Siccinio, G. Federici, *Nucl. Fusion* **2021**, *61*, 126057.
[26] N. Asakura, K. Hoshino, Y. Homma, Y. Sakamoto, *Nucl. Mater. Energy* **2021**, *26*, 100864.
[27] D. Tskhakaya, S. Kuhn, *Contrib. Plasma Phys.* **2002**, *42*, 302.
[28] D. Tskhakaya, R. Schneider, *J. Comp. Phys.* **2007**, *225*, 829.
[29] D. Tskhakaya, K. Matyash, R. Schneider, F. Taccogna, *Contrib. Plasma Phys.* **2007**, *47*, 563.
[30] T. Takizuka, M. Hosokawa, K. Shimizu, *J. Nucl. Mater.* **2003**, *313*, 1331.
[31] T. Takizuka, *Plasma Sci. Technol.* **2011**, *13*, 316.
[32] T. Takizuka, *Plasma Phys. Cont. Fusion* **2017**, *59*, 034008.
[33] R. J. Kanzleiter, D. P. Stotler, C. F. F. Karney, D. Steiner, *Phys. Plasmas* **2000**, *7*, 5064.
[34] H. Matsuura, Y. Nakao, *Phys. Plasmas* **2006**, *13*, 062507.
[35] H. Matsuura, S. Sugiyama, S. Kajimoto, D. Sawada, Y. Nishimura, Y. Kawamoto, *Plasma Fusion Res.* **2016**, *11*, 1403105.
[36] H. Matsuura, Y. Kawamoto, S. Sugiyama, S. Kajimoto, *IEEE Trans. Plasma Sci.* **2018**, *46*, 6.
[37] S. Sugiyama, H. Matsuura, D. Uchiyama, *Phys. Plasmas* **2017**, *24*, 092517.
[38] S. Sugiyama, H. Matsuura, T. Goto, T. Nishitani, M. Isobe, K. Ogawa, *Plasma Fusion Res.* **2019**, *14*, 3403123.
[39] S. Sugiyama, T. Nishitani, H. Matsuura, M. Isobe, K. Ogawa, T. Tanaka, S. Yoshihashi, A. Uritani, M. Osakabe, *Nucl. Fusion* **2020**, *60*, 076017.
[40] K. Kimura, H. Matsuura, Y. Kawamoto, T. Oishi, M. Goto, K. Ogawa, T. Nishitani, M. Isobe, M. Osakabe, *Rev. Sci. Instrum.* **2021**, *92*, 053524.
[41] M. H. Hughes, D. E. Post, *J. Comp. Phys.* **1978**, *28*, 43.
[42] K. Shimizu, *J. Nucl Mat.* **1995**, *220*, 410.
[43] B. A. Trubnikov, *Rev. Plasma Phys.* **1965**, *1*, 105.
[44] K. Shimizu, T. Takizuka, *J. Plasma Fusion Res.* **1995**, *71*, 1135.
[45] M. S. Islam, Y. Nakashima, S. Ishiguro, K. Hoshino, A. Hatayama, H. Hasegawa, M. Sakamoto, *Plasma Fusion Res.* **2021**, *16*, 2403049.
[46] R. Ito, T. Tabata, N. Itoh, K. Morita, T. Kato, H. Tawara, *Data on the Backscattering Coefficients of Light Ions from Solids*, IPP Nagoya University, Nagoya **1985**.
[47] H. Q. Wang, J. G. Watkins, H. Y. Guo, M. Groth, A. E. Jarvinen, A. W. Leonard, J. Ren, D. M. Thomas, J. Boedo, *Phys. Plasmas* **2021**, *28*, 052509.
[48] K. Hoshino, A. Hatayama, N. Asakura, H. Kawashima, R. Schneider, D. Coster, *J. Nucl. Mat.* **2007**, *363*, 539.

**How to cite this article:** D. Umezaki, H. Matsuura, K. Hoshino, *Contrib. Plasma Phys*. **2023**, e202300064. https://doi.org/10.1002/ctpp.202300064